Dear Editors of EarthArXiv,

We submit our manuscript,
“Foreshock Acceleration Linked to Slow Earthquakes Before a Large Earthquake: Implications for Two-Stage Aseismic Processes,”
for consideration as a preprint.
This manuscript was submitted to the journal "Earth, Planets and Space" and now under review.

Author #1: Shukei Ohyanagi, Disaster Prevention Research Institute, Kyoto University, ohyanagi.shukei.82r@st.kyoto-u.ac.jp
Author #2: Yuta Ito, Graduate School of Science, Kyoto University, ito.yuta.82f@st.kyoto-u.ac.jp
Author #3: Kai Koyama, Graduate School of Science, Kyoto University, koyama.kai.73e@st.kyoto-u.ac.jp
Author #4: Tomoaki Nishikawa, Disaster Prevention Research Institute, Kyoto University, nishikawa.tomoaki.2z@kyoto-u.ac.jp

This study analyzes a very recent *M* 6.9 interplate earthquake that occurred in November 2025 in the Japan Trench subduction zone, documenting an exceptionally pronounced and short-term foreshock acceleration immediately preceding the mainshock, together with contemporaneous tectonic tremor bursts detected by the S-net ocean-bottom seismometers. The foreshock acceleration is shown to be statistically unprecedented over a 19-year record, while the tremor activity indicates the progression of slow slip on the plate interface.

Sincerely,
Shukei Ohyanagi

Title: ForeshockAcceleration Linked to Slow Earthquakes Before a Large Earthquake: Implications for Two-StageAseismicProcesses

Author #1: Shukei Ohyanagi, Disaster Prevention Research Institute, Kyoto University, ohyanagi.shukei.82r@st.kyoto-u.ac.jp

Author #2: Yuta Ito, Graduate School of Science, Kyoto University, ito.yuta.82f@st.kyoto-u.ac.jp

Author #3: Kai Koyama, Graduate School of Science, Kyoto University, koyama.kai.73e@st.kyoto-u.ac.jp

Author #4: Tomoaki Nishikawa, Disaster Prevention Research Institute, Kyoto University, nishikawa.tomoaki.2z@kyoto-u.ac.jp

Corresponding author: Shukei Ohyanagi

Abstract

Foreshocks are important for understanding the initiation process of large earthquakes. It has long been suggested that the acceleration of foreshock activity is driven by precursory aseismic fault slip. However, observational evidence supporting this relationship remains limited. Furthermore, while slow earthquakes—diverse low-velocity fault slip phenomena—frequently occur at plate boundaries, their relationship with foreshock acceleration has not been fully elucidated. Here we report the first instance in which both localized, short-term foreshock acceleration and tectonic tremor bursts were directly observed simultaneously in the same region. Prior to the M_{jma} 6.9 interplate earthquake that occurred on November 9, 2025, in the Japan Trench subduction zone off the coast of Iwate, an exceptionally pronounced acceleration of foreshocks was recorded. We quantitatively characterized this exceptional acceleration using an epidemic-type aftershock sequence model with an acceleration term. Using data from ocean-bottom seismometers located directly above the source region, we found that tremor bursts occurred concurrently with this acceleration, spanning a range of approximately 100 km along-strike, including the foreshock source area. This tremor

activity strongly suggests the progression of slow slip along the plate interface. The foreshock activity accelerated sharply starting three days before the mainshock within the asperity that ruptured during the 1968 M_w 7.0 earthquake. In contrast, the nearby tremor activity showed no comparably strong acceleration. Based on these results, we interpret that slow slip accompanied by tremor bursts had been progressing along the plate interface for about one week prior to the mainshock. This slow slip may have promoted accelerating aseismic slip within the asperity (i.e., preslip), leading to the intense foreshock acceleration and the subsequent large earthquake.

Keywords

Foreshock, Slow earthquakes, Tectonic tremor, Slow slip, Earthquake nucleation, Preslip

1 Introduction

Understanding the physical processes that precede large earthquakes is one of the most fundamental challenges in seismology. Foreshock activity, a series of earthquakes occurring before a mainshock, can provide crucial insights into such preparatory processes (e.g., Dodge et al. 1996; Jones and Molnar 1979). Numerical simulations and laboratory experiments suggest that intensive foreshocks preceding mainshocks are driven by accelerating aseismic slip during the mainshock nucleation phase (hereafter referred to as preslip). Rate-and-state friction simulations predict that preslip can trigger foreshock sequences with increasing rates as faults approach dynamic instability (Ampuero and Rubin 2008; Dublanchet 2018). Laboratory stick-slip experiments demonstrate that dynamic failure is preceded by aseismic slip accompanied by increasing acoustic emissions (Dresen et al. 2020; Bolton et al. 2023). However, clear observational evidence of preslip on natural faults remains lacking, despite these theoretical and experimental results.

Although preslip has not been clearly documented, plate boundary faults are known to

host various modes of low-velocity fault slip phenomena. Intense seismic and geodetic observations over the past two decades have revealed slow earthquake activity globally, most of which occurs at plate boundary faults in subduction margins (e.g., Obara and Kato 2016). Slow earthquakes encompass several types of phenomena. Slow slip events (SSEs) produce crustal deformation over timescales of days to months that is detectable only through geodetic measurements. Tectonic tremor is a type of slow earthquake that can be observed seismically. Bursts of tremor activity are usually associated with SSEs (e.g., Rogers and Dragert 2003; Obara et al. 2004; Hirose and Obara 2010). Because offshore SSEs are often difficult to detect due to limitations in seafloor geodetic observations, tremor activity is widely used as a proxy for SSE occurrence.

Recent observations suggest that slow earthquakes are involved in foreshock occurrence. For example, the 2011 M_w 9.0 Tohoku-Oki earthquake was preceded by a month-long SSE (Ito et al. 2013) and migrating foreshocks (Kato et al. 2012), suggesting a possible triggering of the foreshocks by the SSE. However, the relationships between slow earthquakes and the rapid acceleration of foreshock activity

potentially associated with preslip, as well as between slow earthquakes and preslip itself, remain poorly understood owing to limited direct observational evidence. Clarifying this relationship is crucial for understanding earthquake nucleation processes.

On November 9, 2025, a M_{jma} 6.9 interplate earthquake occurred off the coast of Iwate in the Japan Trench subduction zone (Figure 1). Prominent acceleration of foreshock activity was observed prior to the M_{jma} 6.9 mainshock. The region adjacent to the foreshock and mainshock epicentral areas is known to host a wide spectrum of slow earthquakes. Onshore broadband seismic observations have reported the occurrence of very-low-frequency earthquakes (Matsuzawa et al. 2015; Baba et al. 2020), whereas recent developments in the offshore seismic observation network (S-net; Aoi et al. 2020) have revealed detailed tremor activity (Tanaka et al. 2019; Nishikawa et al. 2019, 2023; Sagae et al. 2025). The close spatial proximity between the slow earthquake source region and the area of prominent foreshock activity implies a possible relationship between the two.

In this study, we quantitatively characterize the foreshock acceleration using an epidemic-type aftershock sequence (ETAS) model designed for accelerating seismicity. We then detect tectonic tremors from S-net ocean-bottom seismometer records to compare foreshock and slow earthquake activity. Through these analyses, we discuss how slow earthquakes may have been involved in the rupture nucleation process of the M_{jma} 6.9 mainshock.

2 Methods and Data

2.1 Analysis of Seismicity Acceleration

The epidemic-type aftershock sequence (ETAS) model is a widely used statistical framework for modeling seismic activity (Ogata 1988). In this study, we used the ETAS model with an acceleration term (ETAS-A model) proposed by Koyama and Nishikawa (2025) to quantitatively evaluate the characteristics of accelerating foreshock activity.

The ETAS-A model expresses the earthquake occurrence rate $\square(\square)$ at time $\square$ as follows.

$$\square(\square) = \square + \sum_{\square > \square_{\square}} \frac{\square \exp(\square(\square_{\square} - \square_{\square}))}{(\square - \square_{\square} + \square)^{\square}} + \square(\square) \qquad (1)$$

$$\square(\square) = \frac{\square}{(\square_{\text{end}} - \square + \square)^{\square}} \quad (2)$$

Here, $\square_{\square}$ and $\square_{\square}$denote the magnitude and occurrence time of the i-th earthquake, respectively, and $\square_{\square}$ is the minimum magnitude of earthquakes used in the analysis. In the first term on the left-hand side, $\square$ denotes the stationary background seismicity rate; the second term accounts for aftershock activity due to earthquake-to-earthquake triggering; and the third term, $\square(\square)$,represents time-dependent background seismicity that accelerates toward the end time of the analysis period, $\square_{\text{end}}$.When this time is set to coincide with the occurrence time of the mainshock, the model can represent the acceleration of seismicity toward the mainshock occurrence time. In this model, the target large earthquake is not treated as an event stochastically generated by the nonstationary Poisson process; rather, it is assumed to occur independently through a separate physical process (Koyama and Nishikawa 2025). The functional form of the acceleration term is based on foreshock acceleration observed in earthquake cycle simulations (e.g., Yabe and Ide 2018) and laboratory rock experiments (e.g., Marty et al. 2023). The parameters of the ETAS-A model ($\square$, $\square$,$\square$,$\square$,$\square$,$\square$,$\square$,$\square$) were estimated using the maximum likelihood method.

Based on this model, we define metrics that characterize the acceleration of seismicity. The probability that earthquake i, which occurred at time t_i, was generated by the acceleration term, μ_{acc}, can be calculated as follows (Koyama and Nishikawa 2025).

$$p_{acc} = \frac{\mu(t_i)}{\lambda(t_i)} \times 100\% \quad (3)$$

Hereafter, we refer to this probability as the acceleration probability. In this study, earthquakes with an acceleration probability exceeding 50% are regarded as events attributed to the acceleration term, and their number, N_{acc}, is counted. Furthermore, the median of the time differences between the occurrence times of events attributed to the acceleration term and the end time t_{end} is regarded as a characteristic timescale of the acceleration phenomenon, which we call the half-duration of the acceleration phase, T_{acc}. Acceleration characterized by larger N_{acc} and shorter T_{acc} is interpreted as more pronounced acceleration.

In this analysis, we applied the ETAS-A model to earthquakes with magnitudes of $M_{jma} \geq 3.0$ ($M_0 = 3.0$) that occurred in the northern Japan Trench subduction zone during

the three years preceding the M_{jma} 6.9 mainshock on 9 November 2025 (Figure 1). We used the Japan Meteorological Agency (JMA) earthquake catalog. A minimum magnitude of M_{jma} 3.0 is sufficiently higher than the completeness magnitude in this region. As described below, because the ETAS-A model analysis was extended back to 2001, a relatively large minimum magnitude was adopted. The end time $\square_{end}$ was set to coincide with the occurrence time of the mainshock.

Next, to evaluate how rare the foreshock acceleration observed is, we retrospectively applied the ETAS-A model to past seismicity. Specifically, we shifted the end time of each 3-year time window, $\square_{end}$,backward in time at 1-hour intervals, starting at 17:00 on 9 November 2025, and conducted the analysis until 18:00 on 11 November 2016. The same analysis was also performed for the period from 01:00 on 1 January 2001 to 00:00 on 1 January 2011. In total, the ETAS-A model was applied to an earthquake catalog spanning approximately 19 years. For each time window, we calculated $\square_{acc}$ and $\square_{acc}$,and examined their distributions. The period from 2011 to 2016 was excluded from the analysis to avoid long-term effects of the 2011 Tohoku-Oki earthquake.

2.2 Tectonic Tremor Detection

To detect tectonic tremors off Iwate, we used seismic data from the S-net, a cabled ocean-bottom seismic network along the Japan Trench (Aoi et al. 2020). We selected 20 stations located above the tremor sources. We focused on the period from October 24 to November 11, 2025.

We used the modified envelope cross-correlation method (Mizuno and Ide 2019) to detect tremors. First, three-component seismograms were rotated to horizontal and vertical components based on sensor tilt and orientation information from Takagi et al (2019). We then made envelope waveforms using only horizontal components (Kanasewich 1981). The horizontal component waveforms were demeaned, detrended, and bandpass-filtered between 2 and 8 Hz. The envelope waveform was smoothed by applying a low-pass filter of 0.3 Hz and then resampled at 1 Hz. The envelope waveforms at each station were divided into 300-s time windows with 150-s overlap, and the modified envelope correlation method (Mizuno and Ide 2019) was applied to each window.

We estimated location uncertainty of detected tremors using bootstrapping. We randomly selected cross-correlation functions of different station pairs and performed event location 300 times. The location uncertainty was defined as the median distance of the bootstrap-derived locations from the original location.

The detection results obtained so far include non-tremor signals, such as regular earthquakes, which were removed in the following analysis. Because earthquakes generally have shorter durations than tremors, we removed events with durations shorter than 20 s following Nishikawa et al. (2019, 2023). In addition, we compared the detected events with the JMA earthquake catalog and removed events listed in the earthquake catalog.

To improve tremor catalog quality and reduce potential false positives, we removed events with epicentral uncertainties larger than 10 km, fewer than four stations involved in the location, or estimated durations longer than 250 s. Because tremors are generally

known to occur in swarm-like episodes (e.g., Wech and Creager 2008), we applied spatiotemporal clustering to remove isolated detections. Following Sagae et al. (2025), events were retained in the catalog only if five or more events occurred within a temporal window of 24 h and an epicentral distance of 20 km.

3 Results

Figure 1 shows the acceleration probabilities calculated by the ETAS-A model. Earthquakes with high acceleration probabilities are concentrated around the epicenter of the mainshock (Figure 1a). As shown in Figures 1c and 1d, events with relatively high acceleration probabilities (40% or higher) began to occur about eight days before the mainshock, and events exceeding 50% were observed about three days before. The foreshock activity then rapidly accelerated. The estimated ETAS-A parameters and metrics of the foreshock activity are summarized in Table 1. The number of earthquakes attributed to the acceleration term, $\square_{acc}$, is 34, and the half-duration of the acceleration phase, $\square_{acc}$, is 0.47 days.

Table 1. Estimated parameters and metrics for the ETAS–A model.

Background and aftershock parameters				
□ (events/day)	□	□ (days)	□	□
0.27	1.1	6.0×10^{-4}	6.0×10^{-2}	0.95
Acceleration parameters and metrics				
□ (days)	□	□	$□_{acc}$ (events)	$□_{acc}$ (days)
0.44	15.4	1.9	34	0.47

To quantify how rare the observed foreshock acceleration was, we repeatedly applied the ETAS-A model to seismic activity in the same region while shifting the time window by one hour (Figure 2). As a result, over approximately 19 years, cases in which $\Box_{acc}$ exceeded 30 were associated only with the foreshock acceleration in November 2025, and the proportion was 0.006% (10 out of 166,474 windows). $\Box_{acc}$ for the November 2025 foreshock sequence (more than 30 events) was identified as a clear outlier (Figure 2b). In addition, $\Box_{acc}$ for the November 2025 foreshock sequence was particularly short (less than one day). No similar acceleration of seismic activity was identified within the study period.

The detection results of tremor activity are shown in Figure 3. Tremor bursts began about one week before the mainshock, near 39.9°N, immediately after two earthquakes of M_{jma} 4.6 and M_{jma} 4.4 on November 2, and spread over a region of approximately 50 km in the north–south direction (Figure 3c). These tremors are distributed complementarily to the slip areas (asperities) of past interplate earthquakes with $M_w \geq$ 7.0 (Figure 3a; Yamanaka and Kikuchi 2004). Subsequently, about six days before the

mainshock, a M_{jma} 5.3 earthquake occurred near 39.4°N, and tremor activity became active also on the southern side. By the time of the mainshock, the tremor-active region had expanded to more than 100 km in the north–south direction.

The foreshock activity began to accelerate rapidly about three days before the occurrence of the mainshock (Figures 3b and 3c). It was concentrated within a narrow area inside the asperity of the 1968 M_w 7.0 earthquake (Yamanaka and Kikuchi 2004), within a north–south extent of less than 20 km (Figure 3a). This asperity broadly overlaps with a first-order estimate of the mainshock source area derived from aftershock activity during the first 24 hours following the mainshock (Figure 3a). The intense foreshock activity continued until immediately before the mainshock. In contrast, for tremor activity, no pronounced change in the tremor occurrence rate comparable to the foreshock activity was observed, either over the entire region or near the foreshock source area (Figure 3b).

4 Discussion and Conclusions

This study presents the first observation of extremely pronounced, short-term, and localized foreshock acceleration together with tremor bursts in the same region and during the same period. Given the growing interest in the relationship between slow earthquakes and large earthquakes (e.g., Obara and Kato 2016; Nishikawa et al. 2023), as well as between slow earthquakes and foreshock activity (e.g., Kato et al. 2012; Bouchon et al. 2013), this represents an important observational result. In this section, we discuss the processes that were underway prior to the M_{jma} 6.9 mainshock, based on the observational findings identified in this study.

The activity of tectonic tremor is well known to be a good indicator of the propagation of slow slip (e.g., Rogers and Dragert 2003). In this context, the tremor bursts shown in Figure 3 strongly imply that an SSE was progressing on the plate interface. The tremor bursts began about one week before the mainshock, near 39.9°N, following two M 4-class earthquakes, raising the possibility that these earthquakes triggered the SSE. The slip area of the SSE is inferred to have expanded to approximately 100 km in the north–

south direction by the time of the mainshock.

In contrast, the foreshock activity began to accelerate rapidly about three days before the mainshock and was localized within the asperity of the 1968 M_w 7.0 earthquake. Such foreshock acceleration is commonly observed in rock experiments (e.g., Marty et al. 2023) and earthquake cycle simulations (e.g., Yabe and Ide 2018), where it is associated with preslip within a locked fault patch. Moreover, the analysis using the ETAS-A model demonstrated that this foreshock acceleration cannot be explained by ordinary aftershock cascades. The ETAS-A model extracted seismic activity that deviates from ordinary earthquake-to-earthquake triggering as an acceleration term, suggesting the presence of a background aseismic process that accelerates seismic activity.

Based on the above discussion, we interpret the observed foreshock acceleration to reflect the preslip preceding the M_{jma} 6.9 earthquake (Figure 4). Approximately one week before the mainshock, an SSE accompanied by tremor bursts was progressing

along the plate interface. This SSE may have promoted rupture nucleation within the asperity. The nucleation process likely involved accelerating aseismic slip, which led to intense foreshock acceleration and ultimately to the occurrence of the M_{jma} 6.9 mainshock. These observations suggest a two-stage aseismic process involving an SSE followed by preslip. The fact that foreshock activity accelerated rapidly starting about three days before the mainshock, whereas no comparably pronounced change in tremor activity was observed (Figure 3b), is also consistent with the existence of two distinct processes.

An alternative interpretation, in which a widespread SSE occurring along the plate interface off Iwate may have directly triggered the accelerated foreshock activity, cannot be completely ruled out. However, tremor bursts (and likely associated SSEs) are known to occur frequently off the coast of Iwate—approximately once every few months (Nishikawa et al. 2019, 2023; Sagae et al. 2025)—yet seismicity acceleration as pronounced as that observed in the present study has never been reported. Considering also that the number of earthquakes attributed to the acceleration term ($\square_{acc}$) represents

a clear outlier (Figure 2b), it is more reasonable to interpret the observed acceleration as reflecting a process distinct from ordinary SSEs, specifically preslip preceding large earthquakes.

This study suggests that SSEs and preslip preceding large earthquakes can occur in a temporally and spatially linked manner (Figure 4). Under certain conditions, an SSE may promote preslip within an asperity. Revealing the existence of such a two-stage aseismic process improves our understanding of the physical processes leading to large earthquakes and offers a novel perspective on earthquake rupture initiation.

List of abbreviations

ETAS: Epidemic-Type Aftershock Sequence

ETAS-A model: Epidemic-Type Aftershock Sequence model with an acceleration term

JMA: Japan Meteorological Agency

SSE: Slow slip event

Declarations

Ethics approval and consentto participate

Not applicable.

Consent for publication

Not applicable.

Availability of data and materials

The Japanese Meteorological Agency earthquake catalog can be downloaded from https://www.data.jma.go.jp/eqev/data/bulletin/hypo.html.

The waveform data from the S-net ocean-bottom seismometers (National

Research Institute for Earth Science and Disaster Resilience, 2019) are available at https://www.seafloor.bosai.go.jp/S-net/. The code for the envelope correlation method proposed by Mizuno and Ide (2019) is available at https://github.com/not522/MizunoIde2019. Figures were created using the Generic Mapping Tools (GMT; Wessel et al., 2019; Tian et al., 2025).

Competing interests

The authors declare no competing interests.

Funding

This work was supported by MEXT KAKENHI Grant Number 24K17144, 19H05596, and JST SPRING, Grant Number JPMJSP2110.

Authors' contributions

S.O. conceived the study, organized the research team, and led the detection of tectonic tremors. Y.I. contributed to the analysis design and conducted the detection of tectonic tremors together with S.O. K.K. performed the ETAS-A model analysis together with T.N. T.N. led the

ETAS-A model analysis. All authors discussed the analysis results. S.O. and T.N. wrote the manuscript, and Y.I. and K.K. commented on the manuscript. All authors contributed to the preparation of the figures.

Acknowledgements

The authors have no acknowledgements to declare.

References

Ampuero J-P, Rubin AM (2008) Earthquake nucleation on rate and state faults – Aging and slip laws. Journal of Geophysical Research: Solid Earth 113:. https://doi.org/10.1029/2007JB005082

Aoi S, Asano Y, Kunugi T, Kimura T, Uehira K, Takahashi N, Ueda H, Shiomi K, Matsumoto T (2020) MOWLAS: NIED observation network for earthquake, tsunami and volcano. Earth Planets Space 72:126. https://doi.org/10.1186/s40623-020-01250-x

Baba S, Takeo A, Obara K, Matsuzawa T, Maeda T (2020) Comprehensive Detection of Very Low Frequency Earthquakes Off the Hokkaido and Tohoku Pacific Coasts, Northeastern Japan. J Geophys Res Solid Earth 125:. https://doi.org/10.1029/2019JB017988

Bolton DC, Marone C, Saffer D, Trugman DT (2023) Foreshock properties illuminate nucleation processes of slow and fast laboratory earthquakes. Nat Commun 14:3859. https://doi.org/10.1038/s41467-023-39399-0

Bouchon M, Durand V, Marsan D, Karabulut H, Schmittbuhl J (2013) The long precursory phase of most large interplate earthquakes. Nature Geosci 6:299–302. https://doi.org/10.1038/ngeo1770

Dodge DA, Beroza GC, Ellsworth WL (1996) Detailed observations of California foreshock sequences: Implications for the earthquake initiation process. Journal of Geophysical Research: Solid Earth 101:22371–22392. https://doi.org/10.1029/96JB02269

Dresen G, Kwiatek G, Goebel T, Ben-Zion Y (2020) Seismic and Aseismic Preparatory Processes Before Large Stick–Slip Failure. Pure Appl Geophys 177:5741–5760. https://doi.org/10.1007/s00024-020-02605-x

Dublanchet P (2018) The dynamics of earthquake precursors controlled by effective friction. Geophys J Int 212:853–871. https://doi.org/10.1093/gji/ggx438

Hirose H, Obara K (2010) Recurrence behavior of short-term slow slip and correlated nonvolcanic tremor episodes in western Shikoku, southwest Japan. J Geophys Res 115:B00A21. https://doi.org/10.1029/2008JB006050

Ito Y, Hino R, Kido M, Fujimoto H, Osada Y, Inazu D, Ohta Y, Iinuma T, Ohzono M, Miura S, Mishina M, Suzuki K, Tsuji T, Ashi J (2013) Episodic slow slip events in the Japan subduction zone before the 2011 Tohoku-Oki earthquake. Tectonophysics 600:14–26. https://doi.org/10.1016/j.tecto.2012.08.022

Jones LM, Molnar P (1979) Some characteristics of foreshocks and their possible relationship to earthquake prediction and premonitory slip on faults. Journal of Geophysical Research: Solid Earth 84:3596–3608. https://doi.org/10.1029/JB084iB07p03596

Kanasewich ER (1981) Time sequence analysis in geophysics, 2nd edn. University of Alberta Press, Edmonton

Kato A, Obara K, Igarashi T, Tsuruoka H, Nakagawa S, Hiratta N (2012) Propagation of Slow Slip Leading Up to the 2011 M_w 9.0 Tohoku-Oki Earthquake. Science 335:705–708. https://doi.org/10.1126/science.1215141

Koyama K, Nishikawa T (2025) Global investigation of foreshock acceleration prior to large earthquakes. PREPRINT (Version 1). https://doi.org/10.21203/rs.3.rs-8343941/v1

Marty S, Schubnel A, Bhat HS, Aubrey J, Fukuyama E, Latour S, Nielsen S, Madariaga R (2023) Nucleation of Laboratory Earthquakes: Quantitative Analysis and Scalings. Journal of Geophysical Research: Solid Earth 128:e2022JB026294. https://doi.org/10.1029/2022JB026294

Matsuzawa T, Asano Y, Obara K (2015) Very low frequency earthquakes off the Pacific coast of Tohoku, Japan. Geophys Res Lett 42:4318–4325. https://doi.org/10.1002/2015GL063959

Mizuno N, Ide S (2019) Development of a modified envelope correlation method based on maximum-likelihood method and application to detecting and locating deep

tectonic tremors in western Japan. Earth Planets Space 71:40. https://doi.org/10.1186/s40623-019-1022-x

Nishikawa T, Ide S, Nishimura T (2023) A review on slow earthquakes in the Japan Trench. Prog Earth Planet Sci 10:1. https://doi.org/10.1186/s40645-022-00528-w

Nishikawa T, Matsuzawa T, Ohta K, Uchida N, Nishimura T, Ide S (2019) The slow earthquake spectrum in the Japan Trench illuminated by the S-net seafloor observatories. Science 365:808–813. https://doi.org/10.1126/science.aax5618

Obara K, Hirose H, Yamamizu F, Kasahara K (2004) Episodic slow slip events accompanied by non-volcanic tremors in southwest Japan subduction zone. Geophysical Research Letters 31:2004GL020848. https://doi.org/10.1029/2004GL020848

Obara K, Kato A (2016) Connecting slow earthquakes to huge earthquakes. Science 353:253–257. https://doi.org/10.1126/science.aaf1512

Ogata Y (1988) Statistical models for earthquake occurrences and residual analysis for point processes. Journal of the American Statistical association 83: 9–27. https://doi.org/10.1080/01621459.1988.10478560

Rogers G, Dragert H (2003) Episodic Tremor and Slip on the Cascadia Subduction Zone: The Chatter of Silent Slip. Science 300:1942–1943. https://doi.org/10.1126/science.1084783

Sagae K, Kano M, Yabe S, Uchide T (2025) Machine Learning-Based Detection and Localization of Tectonic Tremors in the Japan Trench. Journal of Geophysical Research: Solid Earth 130:e2025JB031348. https://doi.org/10.1029/2025JB031348

Takagi R, Uchida N, Nakayama T, Ryosuke A, Ishigami A, Okada T, Nakamura T, Shiomi K (2019) Estimation of the Orientations of the S-net Cabled Ocean-Bottom Sensors. Seismological Research Letters 90:2175–2187. https://doi.org/10.1785/0220190093

Tanaka S, Matsuzawa T, Asano Y (2019) Shallow Low-Frequency Tremor in the Northern Japan Trench Subduction Zone. Geophys Res Lett 46:5217–5224. https://doi.org/10.1029/2019GL082817

Wech AG, Creager KC (2008) Automated detection and location of Cascadia tremor. Geophysical Research Letters 35:2008GL035458. https://doi.org/10.1029/2008GL035458

Yabe S, Ide S (2018) Variations in precursory slip behavior resulting from frictional heterogeneity. Prog Earth Planet Sci 5:43. https://doi.org/10.1186/s40645-018-0201-x

Yamanaka Y, Kikuchi M (2004) Asperity map along the subduction zone in northeastern Japan inferred from regional seismic data. Journal of Geophysical Research: Solid Earth 109:. https://doi.org/10.1029/2003JB002683

Figure legends

Figure 1. Foreshock acceleration preceding the M_{jma} 6.9 earthquake that occurred on 9 November 2025 in the northern Japan Trench subduction zone. (a) Epicentral distribution of earthquakes used in the ETAS-A model analysis. Circles indicate earthquake epicenters, and colors represent acceleration probability. The red star marks the M_{jma} 6.9 mainshock. The black polygon outlines the analysis region. The solid line with triangles indicates the subduction plate boundary. (b–d) Magnitude–time diagrams and temporal changes in the cumulative number of events within the analysis region.

Figure 2. Statistical characteristics of the ETAS-A model results. The ETAS-A model was applied to earthquake data spanning approximately 19 years, from January 2001 to December 2010 and from August 2016 to November 2025. (a) Distributions of the number of events attributed to the acceleration term $\square_{acc}$ and the half-duration of the acceleration phase $\square_{acc}$. Colors indicate the end year of each analysis window and are shown only to identify the temporal origin of individual windows; no temporal trend is implied. (b) Frequency distribution of $\square_{acc}$.

Figure 3. Comparison of foreshock activity and tectonic tremor activity. (a) Epicentral distributions of foreshocks and tectonic tremors. Small stars indicate epicenters of earthquakes that occurred within 16 days before the mainshock, with colors showing acceleration probability. The large red star marks the epicenter of the mainshock. Small circles indicate tremor epicenters, with colors representing tremor duration. Cross symbols show the locations of S-net ocean-bottom seismometers used for tremor detection. Light yellow areas show the slip distributions of past interplate earthquakes with $M_w \geq 7.0$, corresponding to asperities (Yamanaka & Kikuchi, 2004). The light red area indicates a first-order estimate of the source region of the mainshock, defined as the minimum polygon containing 90% of the aftershocks within 24 hours after the mainshock. Gray solid lines indicate depth contours of the upper surface of the Pacific plate at 10 km intervals. (b) Temporal changes in the cumulative counts of earthquakes and tremors. (c) Spatiotemporal distribution of earthquakes and tremors. Gray stars and circles indicate earthquakes and tremors after the mainshock, respectively.

Figure 4. Schematic illustration of the two-stage aseismic processes preceding the mainshock. Approximately one week before the mainshock, slow slip accompanied by tremor bursts occurred. Subsequently, about three days before the mainshock, accelerating aseismic slip (preslip) developed within the asperity that ruptured during the M_w 7.0 earthquake in 1968. This preslip triggered the pronounced foreshock acceleration.

Figure 1

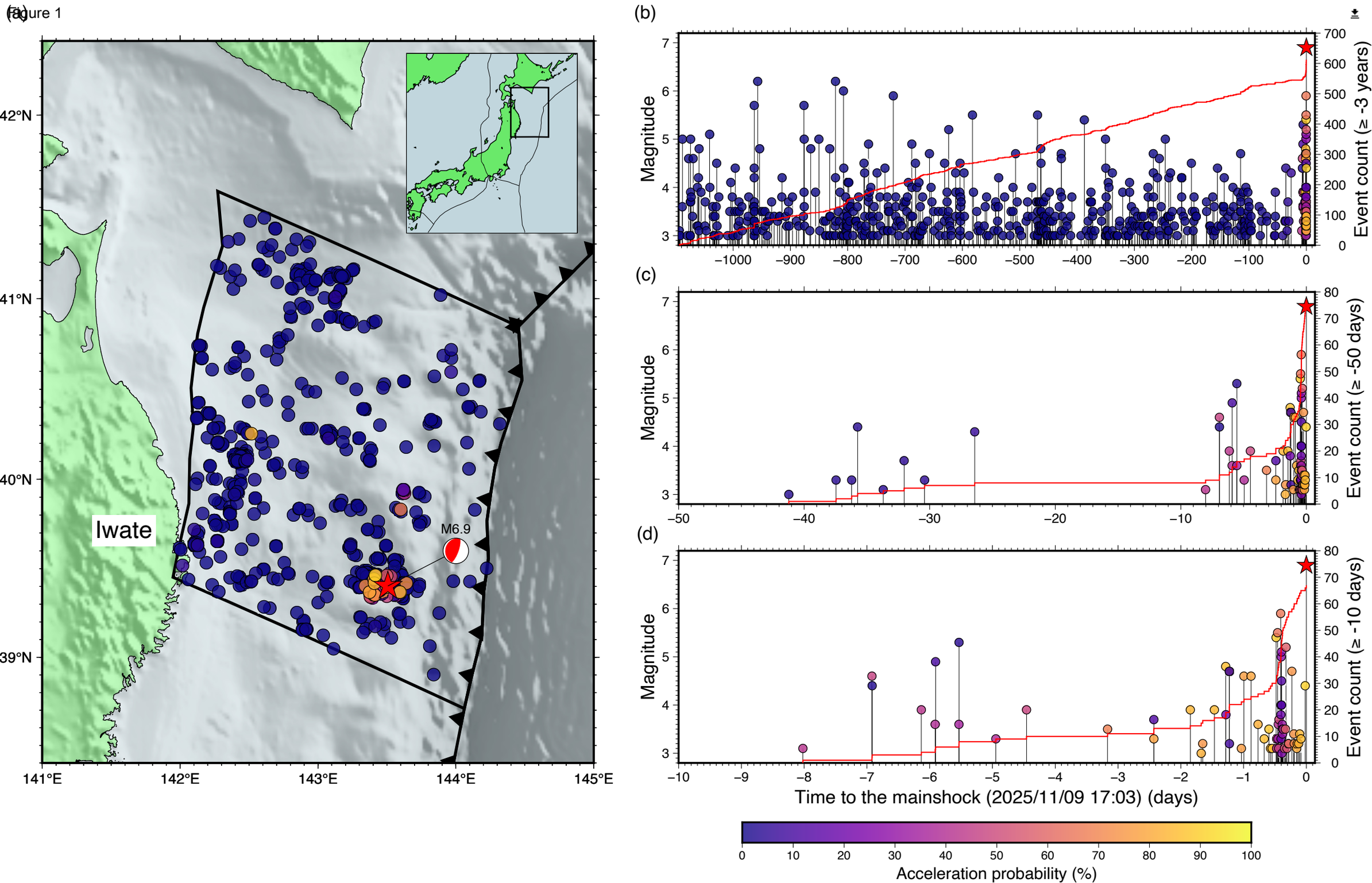
(a)
42°N
41°N
40°N
39°N
141°E
142°E
143°E
144°E
145°E
Iwate
M6.9
(b)
Magnitude
Event count (≥ -3 years)
−1000
−900
−800
−700
−600
−500
−400
−300
−200
−100
0
(c)
Magnitude
Event count (≥ -50 days)
−50
−40
−30
−20
−10
0
(d)
Magnitude
Event count (≥ -10 days)
−10
−9
−8
−7
−6
−5
−4
−3
−2
−1
0
Time to the mainshock (2025/11/09 17:03) (days)
0
10
20
30
40
50
60
70
80
90
100
Acceleration probability (%)

Figure 2

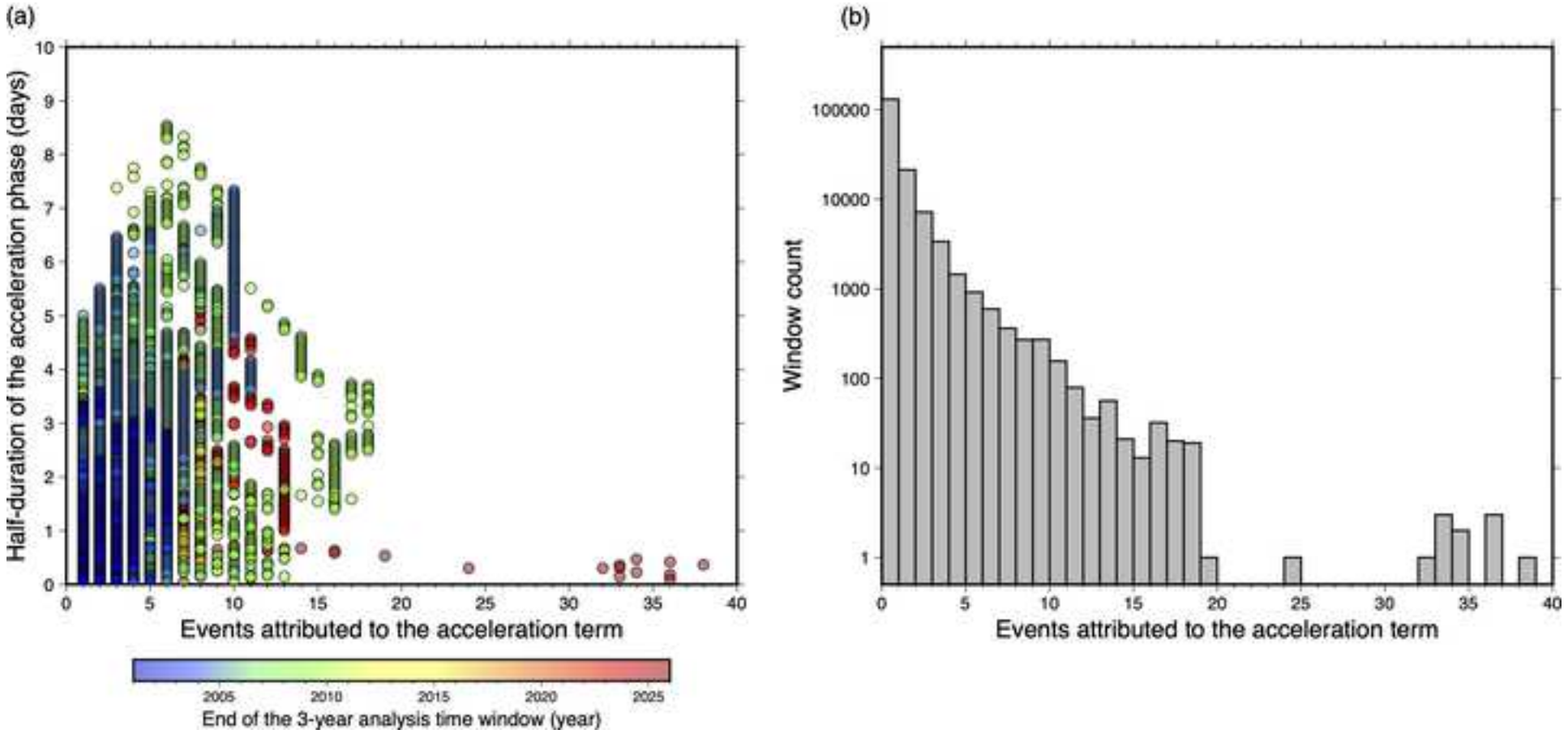

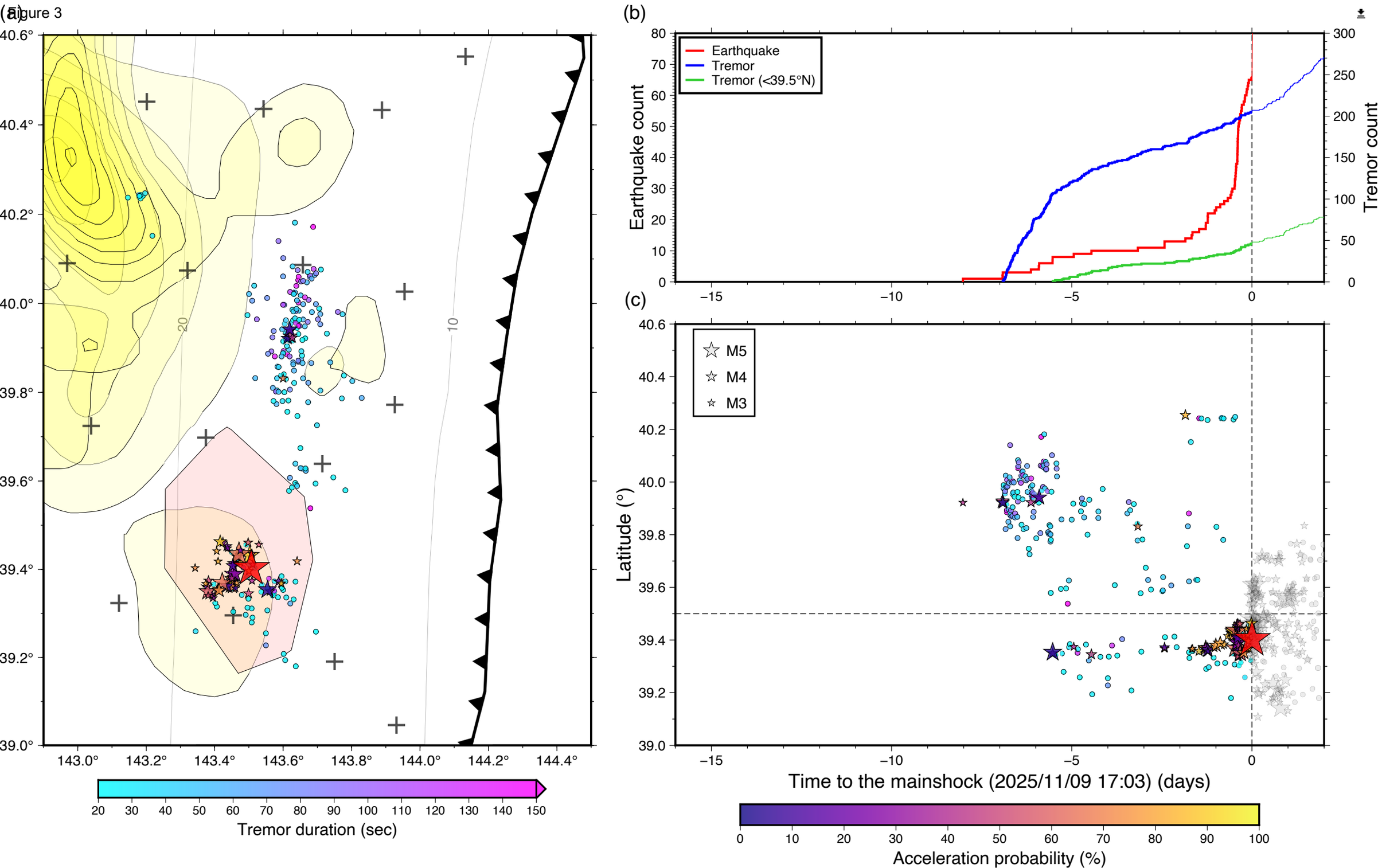
(a)
40.6°
40.4°
40.2°
40.0°
39.8°
39.6°
39.4°
39.2°
39.0°
143.0°
143.2°
143.4°
143.6°
143.8°
144.0°
144.2°
144.4°
20
10
20 30 40 50 60 70 80 90 100 110 120 130 140 150
Tremor duration (sec)
(b)
Earthquake
Tremor
Tremor (<39.5°N)
Earthquake count
Tremor count
(c)
M5
M4
M3
Latitude (°)
Time to the mainshock (2025/11/09 17:03) (days)
0 10 20 30 40 50 60 70 80 90 100
Acceleration probability (%)

Figure 4

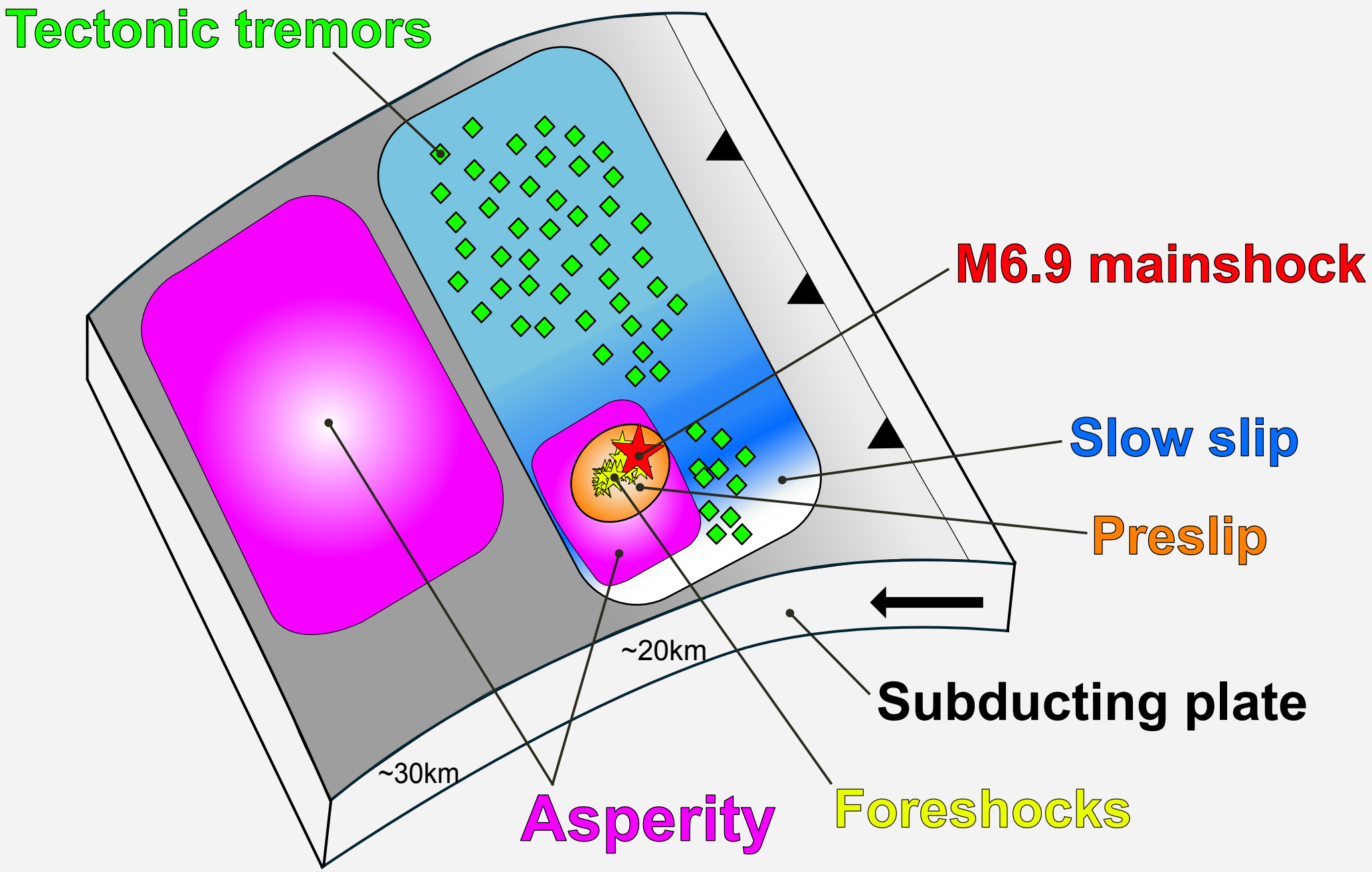
Tectonic tremors
M6.9 mainshock
Slow slip
Preslip
~20km
~30km
Subducting plate
Asperity
Foreshocks

Graphical Abstract (JPEG, PNG or SVG file - 920x300 pixels)